AIAA JOURNAL
Vol. 43, No. 5, May 2005

Synthetic Jets in Crossflow

Ivana M. Milanovic*
University of Hartford, West Hartford, Connecticut 06117
and
K. B. M. Q. Zaman†
NASA John H. Glenn Research Center at Lewis Field, Cleveland, Ohio 44135

Results of an experimental investigation on synthetic jets, with and without crossflow, from orifices of different geometry are presented. Jet Reynolds number up to 2.3×10^4 and Stokes number up to 400 are covered. For the round orifice, in the absence of crossflow, the threshold for formation of the synthetic jet is found to be at a stroke length, $L_0/D \approx 0.25$. Above $L_0/D \approx 5$, the profiles of normalized centerline mean velocity appear to become invariant. It is reasoned that the limiting behavior at high L_0/D is related to the phenomenon of saturation of impulsively generated vortices. For the synthetic jet in crossflow (SJCF), distributions of mean velocity, streamwise vorticity, as well as turbulence intensity are found to be similar to those of a steady jet-in-crossflow (JICF). A pair of counter-rotating streamwise vortices, corresponding to the bound vortex pair of the steady case, is clearly observed. Mean velocity field, for the case of normal injection, exhibits a "dome" of low-momentum fluid pulled up from the boundary layer, and the entire domain is characterized by high turbulence. When the maximum velocity during the discharge stroke of a SJCF equals the exit velocity of a JICF, the penetration of the two are found to be comparable for a given crossflow. Other orifice geometries included a tapered, a pitched, and a cluster of nine, all having the same cross-sectional area at the exit. The flowfield from the cluster, when viewed a few equivalent diameters downstream, resembles that from the single orifice. However, jet penetration is somewhat lower as a result of increased mixing of the distributed jets with the crossflow. Instead of the dome of low-momentum fluid, a pitched SJCF is characterized by a core of high-momentum fluid. Its penetration is the lowest, as expected. The trajectory of the SJCF from a single orifice, normal or pitched, is well represented by the power function correlation available for a JICF.

Nomenclature

A	=	rms voltage input to loudspeaker
D	=	orifice diameter, cm
f	=	forcing frequency, Hz
J	=	momentum-flux ratio, $= (V_{\max}/U_\infty)^2$
L_0	=	stroke length, $L_0 = \int_0^{T/2} v_0(t)\,\mathrm{d}t$
Re	=	Reynolds number, $Re = \bar{V}D/\nu$, $\bar{V} = 2V_0$
S	=	Stokes number, $= \sqrt{(2\pi f D^2/\nu)}$
T	=	forcing period, $= 1/f$
t	=	time
U, V, W	=	mean velocity in streamwise, normal, and spanwise directions
u', v', w'	=	turbulence intensity in streamwise, normal, and spanwise directions
u'_f	=	fundamental rms intensity at the forcing frequency
$V_{\max}$	=	maximum velocity during discharge phase
V_0	=	velocity during discharge phase of the cycle averaged over entire period, $= \frac{L_0}{T} = f\int_0^{T/2} v_0(t)\,\mathrm{d}t$
$\bar{V}$	=	average velocity during discharge phase of the cycle $(= 2V_0)$
$v_0(t)$	=	velocity at exit center of orifice (at $x = y = z = 0$)
x, y, z	=	Cartesian coordinates in streamwise, normal, and spanwise directions (Fig. 1)
$y_{\max}$	=	jet penetration denoted by location of u'_f peak
α	=	pitch angle, between orifice axis and test-section floor
ν	=	kinematic viscosity

Subscripts

c	=	centerline
j	=	jet
∞	=	cross stream

Presented as Paper 2003-3714 at the 33rd AIAA Fluid Dynamics Conference, Orlando, FL, 24 June 2003; received 20 August 2003; revision received 22 October 2004; accepted for publication 15 November 2004. This material is declared a work of the U.S. Government and is not subject to copyright protection in the United States. Copies of this paper may be made for personal or internal use, on condition that the copier pay the $10.00 per-copy fee to the Copyright Clearance Center, Inc., 222 Rosewood Drive, Danvers, MA 01923; include the code 0001-1452/05 $10.00 in correspondence with the CCC.

*Assistant Professor, Mechanical Engineering Department. Member AIAA.

†Aerospace Engineer, Propulsion Systems Division. Associate Fellow AIAA.

I. Introduction

ACTIVE flow control for enhancing propulsive and aerodynamic performance of an aircraft, over a wide range of operating conditions, is of considerable current interest. Potential benefits include alleviation of separation in inlets and ducts, stall margin improvement for turbomachinery, mixing enhancement in jet exhausts and combustors, lift augmentation, and drag reduction for wings as well as noise suppression. Most flow control techniques such as vortex-generating jets, steady or pulsed suction, bleed and oscillatory blowing require a fluid source and accompanying support hardware. In recent research synthetic jets have emerged as a promising technique because they introduce flow perturbation without a net mass injection. Thus, there is no requirement for bleed fluid and minimal demand for additional hardware.

A synthetic jet is created from the ambient fluid by impressing an oscillating pressure gradient across an orifice. Suction pressure entrains the fluid into the orifice and during the discharge phase flow separates at the edges forming a shear layer. The vortex sheet then rolls up and advects away under its own induced velocity. Consequently, a net momentum is transferred to the surrounding fluid even though the net mass flux is zero. Discrete vortical structures

found near the jet exit develop instability followed by vortex core breakdown and the emergence of a fully developed turbulent jet.[1]

A synthetic jet can be generated by a cavity-membrane configuration attached to the jet orifice. Forced oscillatory motion of the membrane, placed on a surface of the cavity, imposes the oscillatory pressure on the orifice. This results in the alternating entrainment and ejection from the orifice causing the formation of the synthetic jet. The pertinent phenomenon of acoustics generating a flow in the presence of a solid surface, or "acoustic streaming," has been well known and studied by aeroacousticians in the past[2,3] as well as lately.[4] However, Ref. 1 and a number of other investigations cited in the following have uncovered the potential of this phenomenon to be a useful flow control tool.

Numerous studies addressed the fundamentals and application of synthetic jets. We touch upon only a few, and the list is by no means exhaustive. Several experiments have noted the resemblance of synthetic jets to continuous jets,[1,5–7] and direct comparison at same Reynolds number[8,9] confirmed self-similar velocity profiles in the asymptotic regions. However, in the initial development region synthetic jets have been found to grow both in width and volume flux more rapidly as a result of the vigorous vortical structures. When applied to flows in various propulsion components, synthetic jets have been shown to produce beneficial effects.[8–17] Specifically, they have been demonstrated to improve lift and drag of bluff bodies,[14] produce desirable vectoring effects on primary jets,[13] delay stall on airfoils,[8] enhance fuel-air mixing,[15] reduce losses and increase the volume flow rate in internal duct flow,[16] and diminish blade-vortex-interaction noise.[17] There are ongoing efforts to achieve high-amplitude perturbations from compact and rugged designs so that the technique could be brought to practical application.[18–20]

In terms of basic research, although extensive work has been done on the structure and dynamics of an isolated synthetic jet, its behavior in a crossflow [synthetic jet in crossflow (SJCF)] has been addressed in relatively few investigations. Virtually all applications would involve a crossflow that is to be "controlled." For a given synthetic jet, the effect of varying crossflow velocity (i.e., momentum-flux ratio) has not been studied systematically. Also, although round or rectangular orifices were the subjects of previous studies, in applications the orifice geometry could often be complex involving pitch and yaw and cluster of orifices. A few previous studies considered complex orifice configurations.[21–27] Furthermore, detailed flowfield information including vorticity and turbulent stresses, useful for simulation and development of models, is also lacking. Finally, most previous works involved relatively low Reynolds number jets, as noted in Ref. 7, and an exploration at higher Reynolds number was deemed appropriate. These provided the motivation for a further investigation.

The present study is an attempt to address some of the cited issues. Wind-tunnel experiments are carried out using hot-wire anemometry. The synthetic jet (SJ) is produced by a cavity-loudspeaker configuration. The characteristics of the SJs, from orifices of different geometry with and without the crossflow, are studied. In the following, results on the parametric dependence of a basic synthetic jet are first presented. Then the penetration and trajectory of a SJCF are explored and compared with those of a jet in crossflow (JICF). Finally, SJCF from orifices of different geometry are compared with a detailed documentation of the flowfields.

II. Experimental Setup

The experiments were conducted in a NASA Glenn Research Center low-speed wind tunnel with 76×51 cm test section. Synthetic jets were created by a loudspeaker (Altec Lansing 36-cm woofer) housed in a chamber underneath the test section as shown in Fig. 1. The orifices were straight holes cut through a 25.4-cm-diam $\times$ 2.54-cm-thick clear plastic plate that is mounted flush on the test-section floor. Most of the data for round jets pertain to the orifice diameter, $D = 1.91$ cm. Limited data were obtained for diameters of 0.95, 3.81, and 7.62 cm. Other orifice geometries are shown schematically in Fig. 1. These include the following: 1) a cluster of nine each with diameter $d = 0.64$ cm, and spaced $2d$ (or $4d$) apart; 2) a slanted one of diameter $D = 1.91$ cm, pitched at $\alpha = 20$ deg

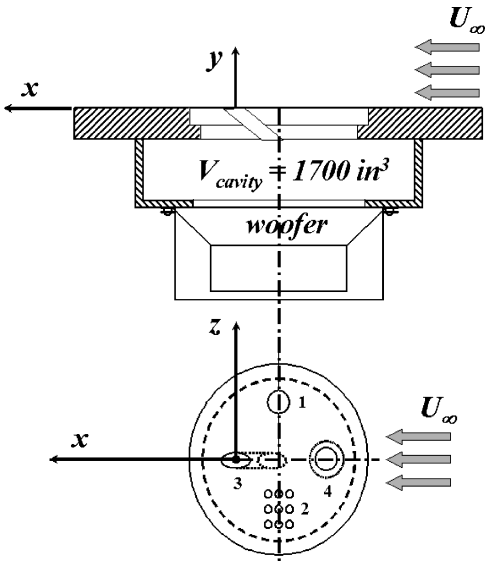

Fig. 1 Experimental setup and orifice configurations: 1) cylindrical, 2) clustered, 3) pitched, and 4) tapered. ($V_{cavity} = 0.0279\ m^3$.)

relative to the floor of the test section; and 3) one tapering from 2.54- to 1.91-cm diam. The equivalent diameter based on the area of cross section through which the flow perturbation discharged into the crossflow was the same for all cases, $D = 1.91$ cm.

Sinusoidal functions were used to drive the woofer, and, at a given frequency, the amplitude of the signal was controlled by varying the input voltage A. For a given input voltage to the loudspeaker, the highest amplitude of the pulsatile flow occurred at the Helmholtz resonance of the chamber. The resonant frequencies for $D = 1.91$- and 7.62-cm orifices, for example, were calculated to be 27.6 and 76.7 Hz, respectively. These were verified to be approximately true by amplitude measurements at the exit of the orifice while varying the frequency. The resonant frequency also increased somewhat when the crossflow was turned on, in agreement with previous observations.[28] In the experiment, however, off-resonant frequencies were often used in order to cover a wide range of the nondimensional stroke length L_0/D. The latter parameter, for a given orifice, depends on the frequency and amplitude.

The measurements were performed by hot-wire anemometry. Two $\times$-wires, one in u–v and the other in u–w configuration, were used for flow mapping in the crossflow plane. The probes were stepped through the same grid points allowing the measurement of all three components of mean velocity and turbulence intensity. The v and w data were corrected for error introduced by u gradients and finite separation of the sensors in each probe. Further details of the measurement procedures can be found in earlier publications.[29] The uncertainty in the normalized u velocity is estimated to be within 2% and that in ω_x to be 20%. A single element of the u-w wire, with appropriate calibration, was used to measure the velocity characteristics at the exit of the orifice. The origin of the coordinate system is located at the center of the orifice as illustrated in Fig. 1. The cross-stream direction (parallel to the tunnel flow) is denoted by x, the direction normal to the tunnel floor is denoted by y, and the spanwise direction by z. Most of the measurements with the SJCF were done for a cross-stream velocity of $U_\infty = 6.1$ m/s. The approach boundary layer was turbulent with a thickness about 60% of the orifice diameter.[29] The Reynolds number based on momentum thickness was about 560.

III. Results

Time traces from the single hot wire are shown in Fig. 2 for various vertical locations on the axis of the orifice, without the crossflow ($U_\infty = 0$). For illustration purposes the traces are staggered successively by one major ordinate division. Near the orifice, flow is reversed during the suction half of the cycle. Velocity readings however are positive throughout the cycle as a result of the directional insensitivity of hot wire. The "rectification" is clearly

seen at $y/D = 0.2$, where the part of the cycle involving smaller amplitudes represents the reverse suction flow. With increasing axial distance the signal during the discharge part of the cycle becomes dominant. The rectification is practically gone at $y/D = 0.5$, and the velocity is positive everywhere at $y/D = 1.0$. The hot-wire rectification is no longer a problem above $y/D \approx 1.0$ and, with the crossflow on, downstream of $x/D \approx 1.0$. As elaborated next, the hot-wire trace from the discharge phase, measured at the smallest y, is utilized to calculate the characteristic velocity.

The properties of the SJ are determined using Smith and Glezer's[1] definition:

$$V_0 = \frac{L_0}{T} = f \int_0^{T/2} v_0(t)\, \mathrm{d}t \tag{1}$$

where V_0, a characteristic velocity, is the integrated value over the discharge half of the cycle and averaged over the entire period. Alternatively, the average velocity during the discharge, $\bar{V} = 2V_0$, has also been used as velocity scale.[4] The stroke length L_0 is the equivalent length of a slug of fluid expelled during the discharge. To evaluate $\bar{V}$ and L_0, the time traces were phase averaged using the signal to the loudspeaker as reference.

Figures 3a and 3b illustrate sample phase-averaged traces with the probe at $y/D = 0.2$ and $z/D = 0$. Results are shown for a) various radial locations x/D without the crossflow and b) the exit center while varying U_∞. It can be seen in Fig. 3a that the traces are practically identical for different radial locations and deviation occurs only when the probe is drawn close to the edge of the orifice. The larger peak on the right represents the discharge half of the cycle. The peak amplitude of the trace during this half together with the trough in the middle are utilized to estimate $\bar{V}$ and L_0, assuming a sinusoidal function. The quantities $\bar{V}$ and L_0 are thus approximations. Most previous studies also used hot wire and involved similar procedure. The parameters for representative cases of the study are listed in Table 1.

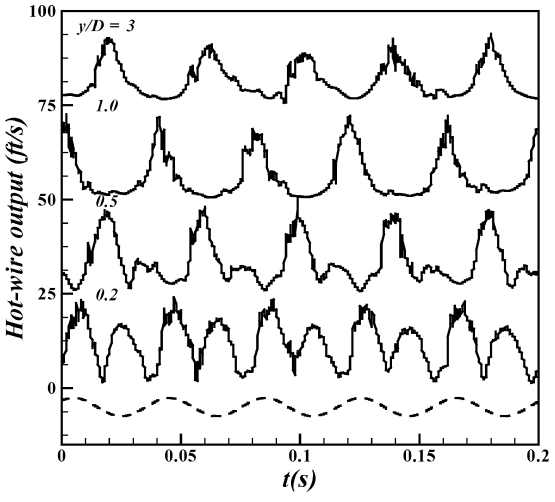

Fig. 2 Hot-wire output at various vertical locations for $D = 1.91$ cm cylindrical orifice: $x/D = 0$, $z/D = 0$, $f = 25$ Hz, $A = 9.6$ V, and $U_\infty = 0$. Dashed curve for sample signal to the woofer. (Ordinate range: 30.5 m/s.)

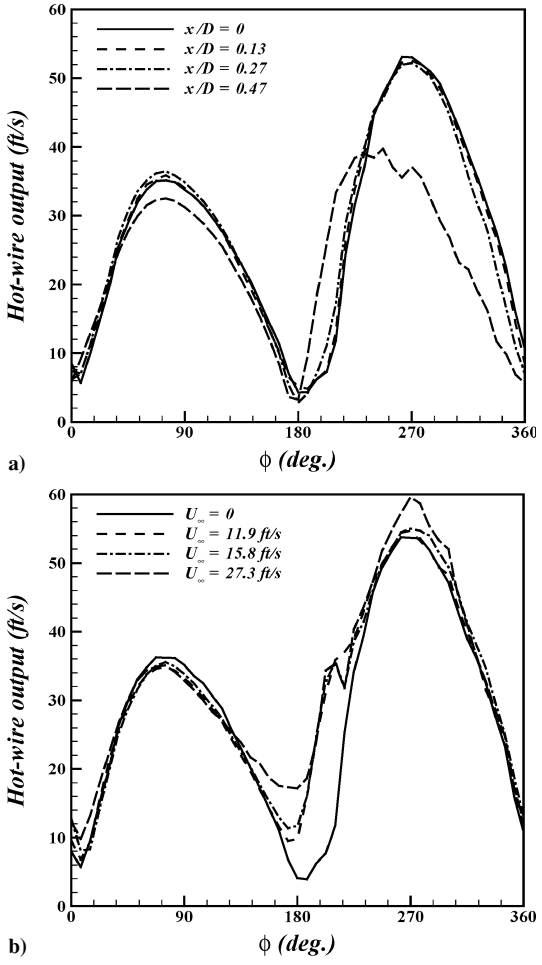

Fig. 3 Phase-averaged hot-wire output at exit of $D = 0.75$-in. orifice: $y/D = 0.2$, $z/D = 0$, $f = 25$ Hz, and $A = 9.6$ V. Measurements a) at indicated radial (x/D) locations with $U_\infty = 0$ and b) at $x/D = 0$ for indicated values of U_∞. (Ordinate range: 18.3 m/s.)

Table 1 Operating parameters for SJs from round orifices

Case	D, cm	f, Hz	A, Vrms	$\bar{V}$, m/s	L_0/D	Re	Re/S^2
1	1.91	12.5	0.67	0.305	0.7	4.06×10^2	0.21
2	1.91	12.5	2.3	1.65	3.46	2.155×10^3	1.10
3	1.91	12.5	5.8	5.06	10.6	6.618×10^3	3.39
4	1.91	12.5	9.6	7.01	14.72	9.154×10^3	4.69
5	1.91	25	0.67	0.98	1.0	1.293×10^3	0.33
6	1.91	25	2.3	3.57	3.8	4.666×10^3	1.19
7	1.91	25	5.8	6.86	7.2	8.976×10^3	2.30
8	1.91	25	9.6	9.48	9.95	12.374×10^3	3.17
9	1.91	50	0.67	0.40	0.2	5.32×10^2	0.07
10	1.91	50	2.3	1.37	0.7	1.8×10^3	0.23
11	1.91	50	4.6	3.02	1.58	3.956×10^3	0.51
12	1.91	50	9.6	7.41	3.89	9.686×10^3	1.24
13	1.91	118	6	1.52	0.34	1.978×10^3	0.11
14	0.95	25	9.6	8.38	17.6	5.464×10^3	5.60
15	3.81	38	9.6	7.96	2.7	20.792×10^3	0.88
16	7.62	65	2.3	1.55	0.16	8.114×10^3	0.05
17	7.62	65	9.6	4.39	0.4	22.922×10^3	0.14

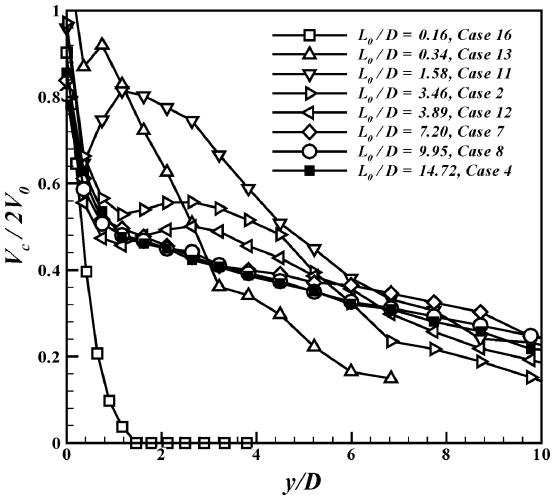

Fig. 4 Normalized centerline velocity profiles for SJs without crossflow ($U_\infty = 0$): $x/D = 0$, and $z/D = 0$. Cases refer to Table 1.

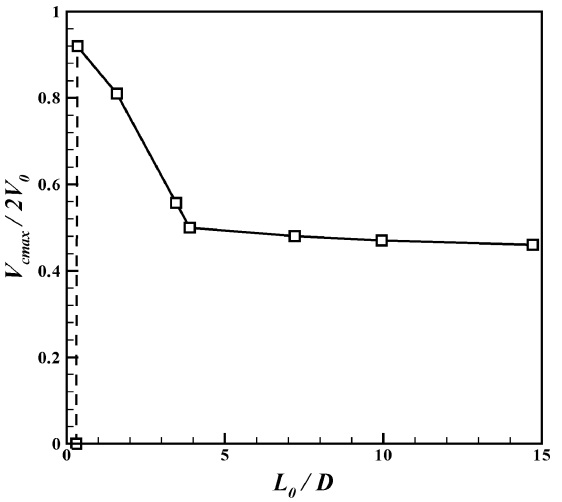

Fig. 5 Peak values of mean velocity V_{cmax} vs L_0/D corresponding to the data of Fig. 4.

With the onset of the crossflow, some changes take place during the rising portion of the signal, as can be seen in Fig. 3b. However, integration of the velocity over the discharge phase made only minor difference in the value of $\bar{V}$ with and without the crossflow. Thus, for the range of U_∞ covered, $\bar{V}$ and L_0 remain practically unchanged at a given frequency and amplitude, and the parameters listed in Table 1 pertain to cases both with and without the crossflow. (Preliminary results of the current investigation were presented in Refs. 30 and 31 with an incorrectly defined velocity scale. Consequently, L_0/D and *Re* values quoted in those two references were off by a factor of 2.)

A. Threshold of Formation and Limiting Behavior of a Round SJ

Normalized centerline velocity profiles without the crossflow are presented in Fig. 4. Mostly because of hot-wire rectification, a positive velocity is read erroneously near the exit, and the data for $y/D < 1$ are disregarded for the rest of the discussion. Clearly, there is a lower threshold of L_0/D at which the velocity profile shows an initial peak and subsequent decay, such as in case 13. Cutoff stroke length is approximately $L_0/D = 0.25$. Below this value a synthetic jet is not formed, and the velocity away from the orifice quickly drops to zero, as in case 16.

The observed threshold for jet formation is compared with a criterion,

$$Re/S^2 > K \tag{2}$$

developed by Utturkar et al.[4] From experimental data K was found to be about 0.16 for axisymmetric synthetic jets. In terms of the stroke length, this can be expressed as

$$L_0/D > \pi K \tag{3}$$

The inequality (3), with the given value of K, yields a lower threshold of about $L_0/D = 0.5$. Thus, in comparison with Ref. 4, the current data exhibit a somewhat lower cutoff stroke length. However, this difference is not pursued further for the following reasons. First, it is increasingly difficult to measure $\bar{V}$ with decreasing amplitudes. Second, orifice thickness-to-diameter ratio also comes into play.[4] This ratio, 1.33 in the present experiment, is smaller than the range (>2) examined in the cited reference. Finally, Stokes S and Reynolds *Re* numbers covered in earlier experiments[2,4,22] spanned from very low values up to 110 and 5000, respectively. In the present work much higher ranges are covered, as listed in Table 1.

A systematic trend in the profiles of Fig. 4 is also observed with increasing L_0/D. The peak velocity decreases progressively, and at large L_0/D (cases 4, 7, and 8) the profiles settle down with very little further change. Thus, there appears to be an upper threshold, $L_0/D \approx 5$, above which the normalized centerline velocity profiles

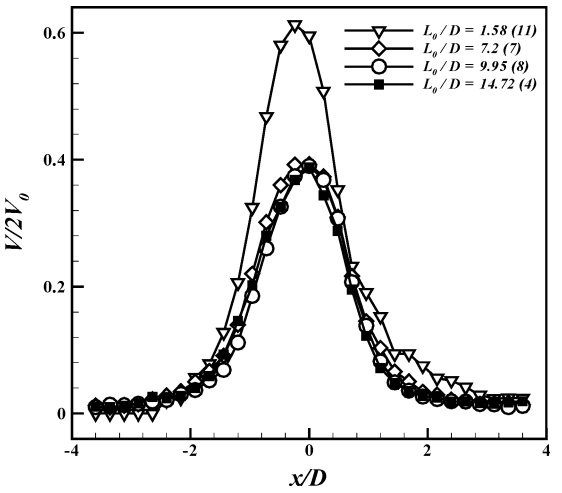

Fig. 6 Normalized velocity profiles for SJs without crossflow ($U_\infty = 0$): $y/D = 4$, and $z/D = 0$. Numbers in parentheses represent cases of Table 1.

become invariant. This is further illustrated in Fig. 5. The peak velocities from Fig. 4 are plotted as a function of L_0/D. (For cases 4, 7, and 8 there are no peaks, and simply the levels at $y/D = 3$ are shown.) The amplitude drops with increasing L_0/D and levels off for $L_0/D > 5$. This limiting behavior is not only characteristic of data at the orifice axis. Radial profiles of mean velocity also become congruent at high L_0/D, as demonstrated in Fig. 6.

It is possible that the upper threshold might have a connection to an observation of Gharib et al.[32] In that work impulsively generated vortex rings with a piston and cylinder arrangement were studied in a water tunnel. Circulation on one-half of the cross-sectional plane containing the jet axis was measured. The total circulation introduced in the flow was a direct function of the piston displacement that corresponds to the stroke length in the present notation. For small L_0/D the total circulation equaled that in the rolled-up vortex. However, with increasing L_0/D, above a certain level, the circulation within the vortex became invariant. For large L_0/D, the excess circulation imparted to the flow appeared as lumps of vorticity trailing the primary vortex. The connection of this observation to the synthetic jets can be as follows.

The dynamics of the synthetic jet are presumably governed by the primary vortex released during each cycle. The effect of any fragmented trailing vortices might be secondary. Thus, if the relative strength of the primary vortex remains unchanged with increasing L_0/D an asymptotic behavior is expected explaining the collapse of

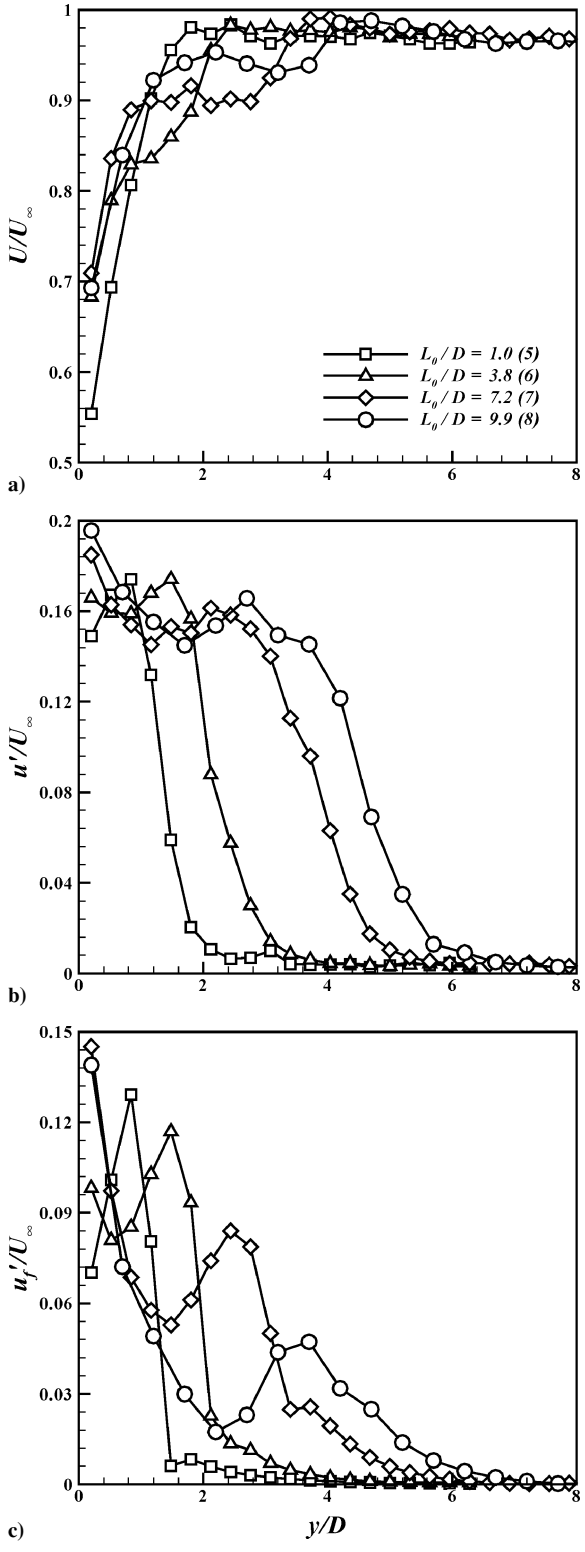

Fig. 7 Mean and fluctuating velocity profiles for SJCF: $x/D = 5$, $z/D = 0$, $f = 25$ Hz, and $U_\infty = 6.1$ m/s. Numbers in parentheses represent cases of Table 1: a) mean velocity, b) turbulence intensity, and c) fundamental (rms) intensity.

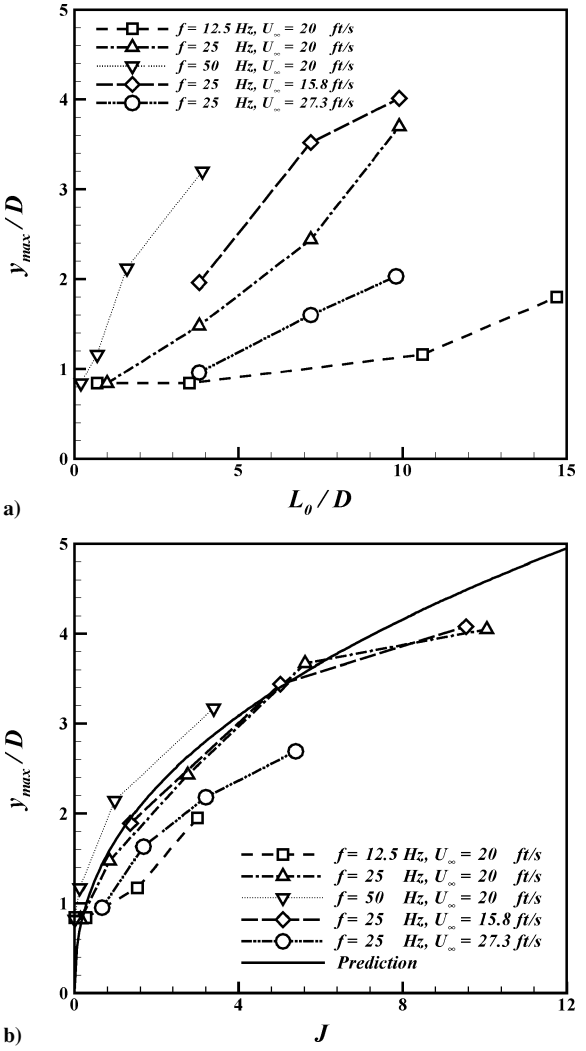

Fig. 8 Vertical location of u'_f peak as a function of a) stroke length L_0/D and b) $J = (V_{max}/U_\infty)^2$: $x/D = 5$, and $z/D = 0$.

mean velocity profiles at high L_0/D. Similar limiting behavior was observed in the thrust augmentation of an ejector subjected to a pulsatile primary flow[33] (Wilson, J., "A Simple Model of Pulsed Ejector Thrust Augmentation," private communication, 2003). However, a full understanding of this upper threshold of saturation and its implication in the design of SJs and in other applications would require further investigation. Although for $L_0/D > 5$ the profiles become congruent, the "strength" of the SJ at a given frequency increases continually with increasing L_0/D. Note also that the limiting formation number of Gharib et al.[32] depends on the shape of the driving signal. The latter is described by a program factor.[26] In the present study only sinusoidal function was used, and the effect of the program factor remains unexplored.

B. Penetration of a Round Synthetic Jet into the Crossflow

Vertical profiles measured five diameters downstream from the orifice are shown in Fig. 7. These data are for a forcing frequency of 25 Hz, cross-stream velocity of 6.1 m/s (20 ft/s), and various amplitudes A. The stroke lengths and relevant case numbers of Table 1 are indicated in the legend. Profiles of mean velocity U are shown in Fig. 7a. Corresponding turbulence intensity u' and fundamental intensity u'_f data are given in Figs. 7b and 7c, respectively. A steplike behavior is developed in the U distributions with increasing L_0/D. The turbulence remains high throughout the region of lower U and decreases sharply as U approaches U_∞. The turbulence is high because it is contributed not only by the fundamental perturbation but also by fluctuations in the separated region. The u'_f data were obtained via spectral analysis of the hot-wire signal. The drop-off in u' coincides with a peak in the u'_f profile, the location of which is denoted as y_{max}. The u'_f peak occurs as a result of a periodic passage of regions of high-velocity gradient, further discussed later with the phase-averaged data. The distance y_{max} provides a convenient measure of the penetration of the SJCF. It will be clear from subsequent data (Sec. III.C) that y_{max} is also closely representative of conventionally defined jet penetration based on mean velocity data.

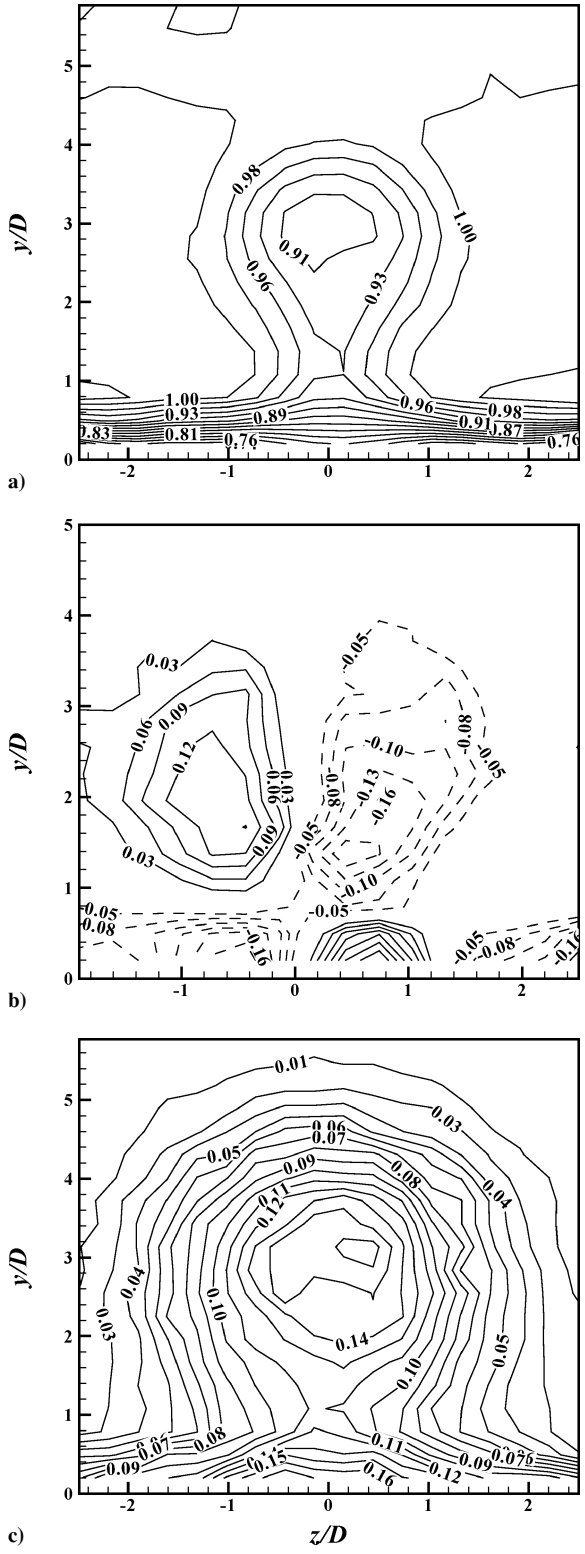

Fig. 9 Contours of streamwise a) mean velocity, b) vorticity, and c) turbulence intensity for SJCF: $x/D = 5$, and $J = (V_{max}/U_\infty)^2 = 6$.

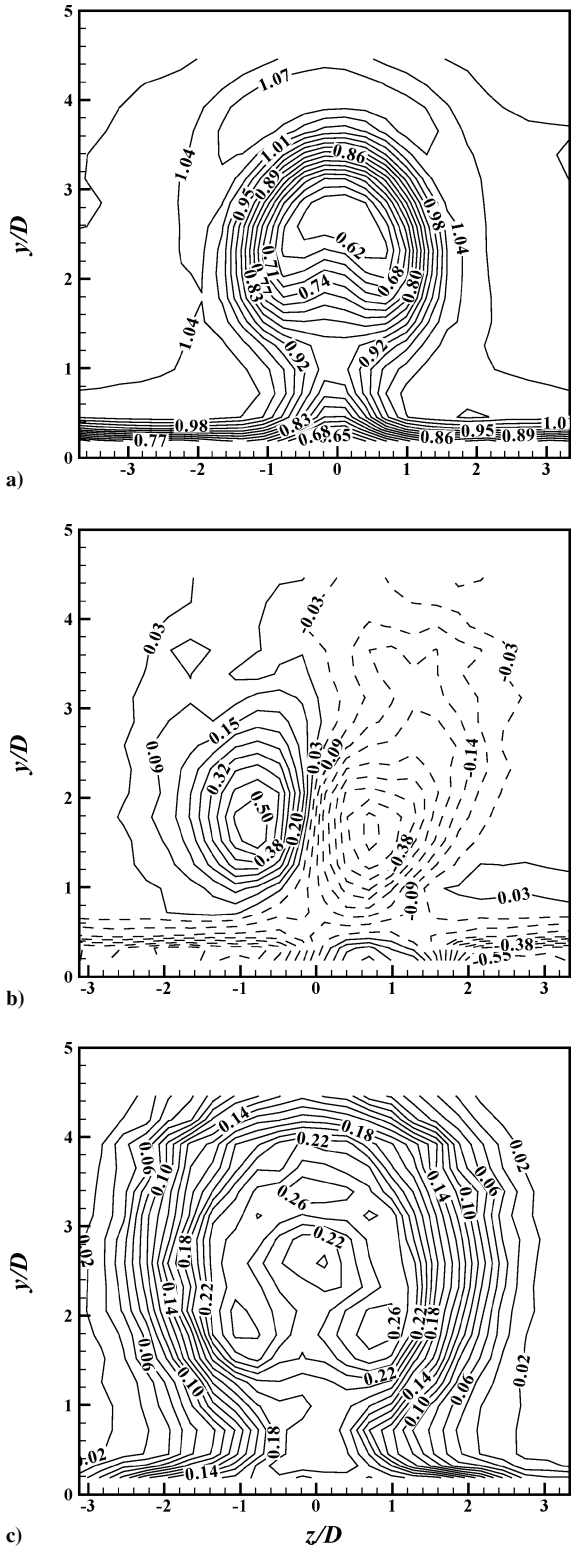

Fig. 10 Contours of streamwise a) mean velocity, b) vorticity, and c) turbulence intensity for JICF: $x/D = 5$, and $J = (V_{jet}/U_\infty)^2 = 6$.

From Fig. 7c it is obvious that with increasing L_0/D, y_{max} increases. That is, a larger stroke length results in a higher penetration of the SJCF.

From a collection of u'_f data as in Fig. 7c, the penetration of SJCF is now examined. In Fig. 8a, y_{max} values for a number of cases are shown as a function of the stroke length. The parameters are indicated in the legends. Clearly, y_{max} is not a unique function of L_0/D. We recall here that the penetration of a JICF depends on the momentum-flux ratio J. For incompressible flow J is equal to the square of the jet-to-cross-stream velocity ratio (V_j/U_∞). This suggests that the penetration of a SJCF should also be dependent upon a momentum-flux ratio. However, the definition of such a ratio is not straightforward because mean exit velocity is zero for the SJCF. After some deliberation, when the data of Fig. 8a were replotted as a function of $(V_{max}/U_\infty)^2$ not only a reasonable collapse occurred but also there was close agreement with the predicted trajectory of

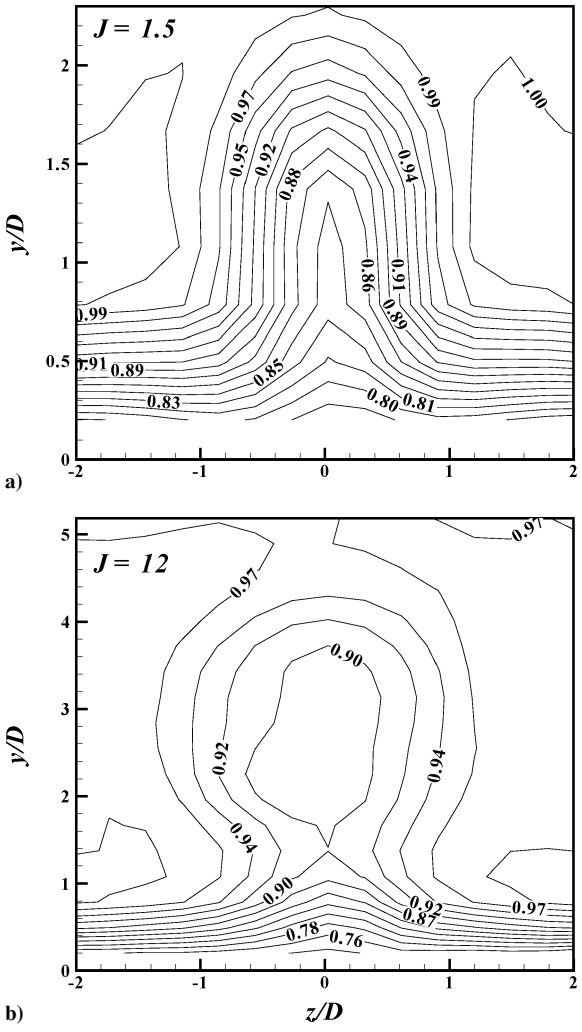

Fig. 11 Streamwise mean velocity contours for SJCF: $x/D = 5$.

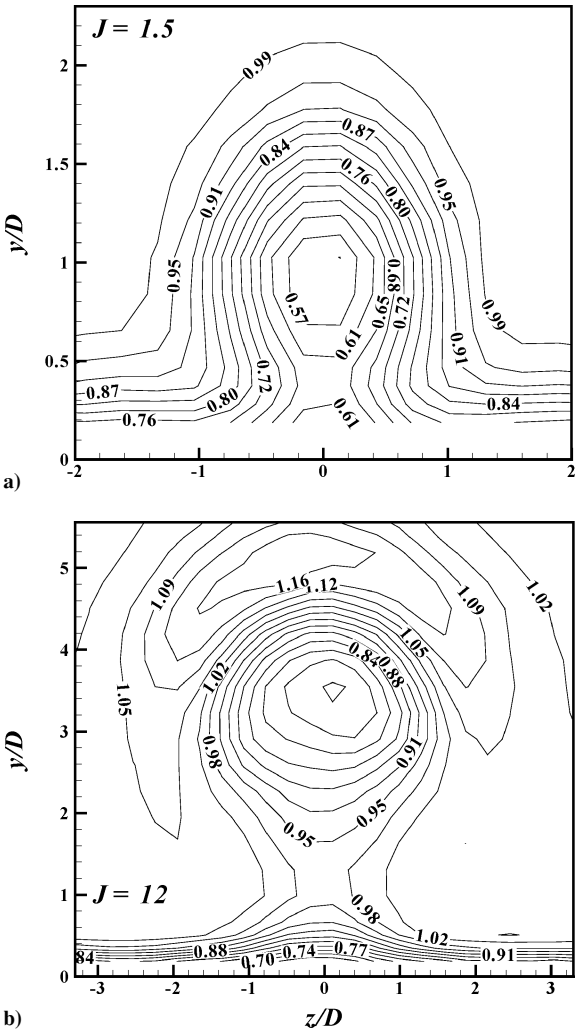

Fig. 12 Streamwise mean velocity contours for JICF: $x/D = 5$.

a JICF. This is shown in Fig. 8b, where the solid curve represents the correlation for the trajectory of a JICF,[34,35]

$$y_{\max}/D = (x/D)^{0.33} J^{0.43} \sin \alpha \tag{4}$$

The aforementioned agreement is dependent upon the adopted definitions of J and $y_{\max}$. Velocity ratio (V_j/U_∞) used for the JICF is substituted by $(V_{\max}/U_\infty)$ for the SJCF. The distance $y_{\max}$, denoting the distance between maximum U and the wall for a JICF, is replaced by the location of u'_f peak for the SJCF. Nevertheless, the applicability of Eq. (4) to SJCF underscores the similarity of the synthetic jet with a steady jet when subjected to a cross-flow. The SJCF trajectories are further compared with Eq. (4) in Sec. III.D.

C. Comparison of Flowfields Between SJCF and JICF

Time-averaged data for a selected SJCF ($L_0/D = 10$ and $J = 6$, case 8 of Table 1) are shown in Fig. 9. Cross-sectional distributions of mean velocity, mean streamwise vorticity, and turbulence intensity measured at $x/D = 5$ are presented. Mean velocity contours in Fig. 9a exhibit a dome of low-momentum fluid. A counter-rotating pair of vortices can be seen in Fig. 9b. The data in Fig. 9c reveal the vigorous turbulent activity and the momentum exchange between the boundary layer and the cross stream. Corresponding data for a JICF, for the same orifice at $(V_j/U_\infty)^2 = 6$, are presented in Figs. 10a–10c. It is apparent that the overall features are similar. The dome of low-momentum fluid, the bound vortex pair as well as the turbulence field, bear direct resemblance. Referring back to the discussion of Fig. 7, one finds that jet penetration is also comparable. However, several differences are also noted. The magnitude of the velocity deficit, the strength of the streamwise vortex pair, as well as the turbulence intensity, are higher in the JICF case. Also, for the SJCF there is a conspicuous vortex pair of opposite sense near the wall underneath the bound vortex pair (Fig. 9b). Only a hint of this can be seen with the JICF (Fig. 10b).

In Figs. 11 and 12 the mean velocity distributions are shown for two more values of J, comparing SJCF with JICF. For the JICF with increasing J, a change in the flowfield topology has been noted in previous experiments.[29,36] Below $J \approx 3$, only a velocity deficit is observed. At higher J, the dome of low-momentum fluid is capped by a kidney-shaped region of high-momentum fluid. This can be seen from the three sets of velocity distributions in Figs. 12 and 10a. We note from the corresponding figures for SJCF (Figs. 11 and 9a) that at each J while the penetration is comparable the high-momentum region is absent.

D. Orifices of Different Geometry

Data for the tapered, slanted, and clustered orifices are compared in this section with that of the single round orifice. Figure 13 shows mean centerline velocity $5D$ away from the exit, without the cross-flow, measured as a function of input voltage to the speaker. For the slanted orifice, the probe was placed on the pitch axis, whereas for the clustered configuration the probe was on the axis of the central hole. One finds that the response to the perturbation is very similar for the cylindrical (with normal injection), tapered, and the clustered cases. A scrutiny reveals that the velocity is slightly higher for the tapered geometry. Comparison of other properties (e.g., streamwise mean and fluctuating velocity distribution at $x/D = 5$, not shown

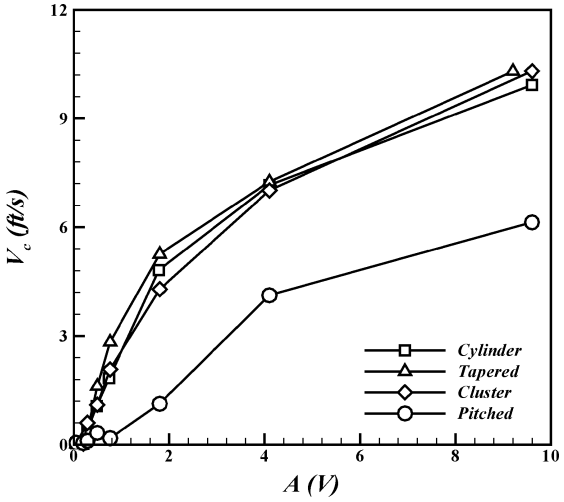

Fig. 13 Mean centerline velocity vs excitation amplitude for SJs from different orifice configurations: $y/D = 5$, $z/D = 0$, $f = 25$ Hz, and $U_\infty = 0$.

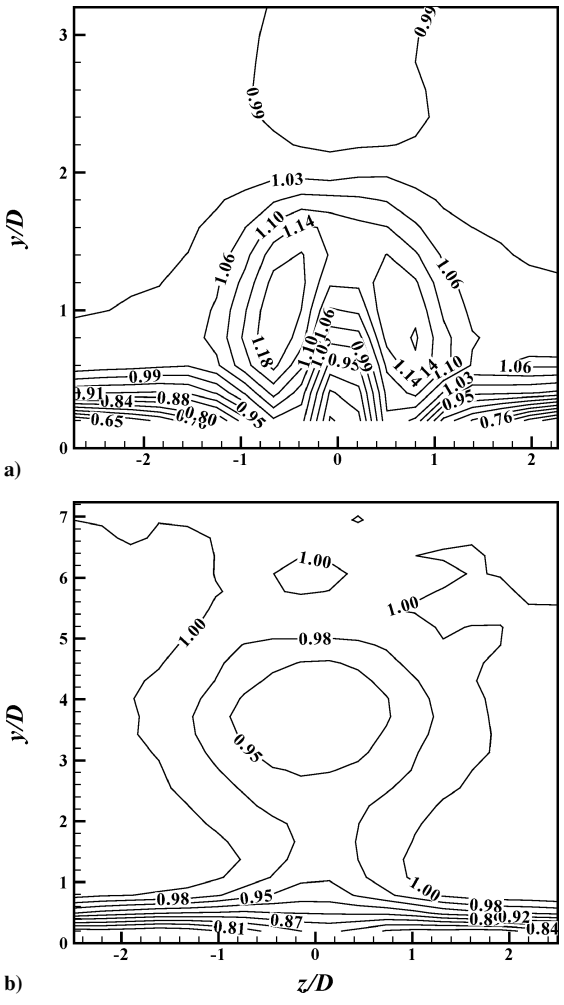

Fig. 14 Streamwise mean velocity contours for SJCF from cylindrical orifice: a) $x/D = 0.5$ and b) $x/D = 10$.

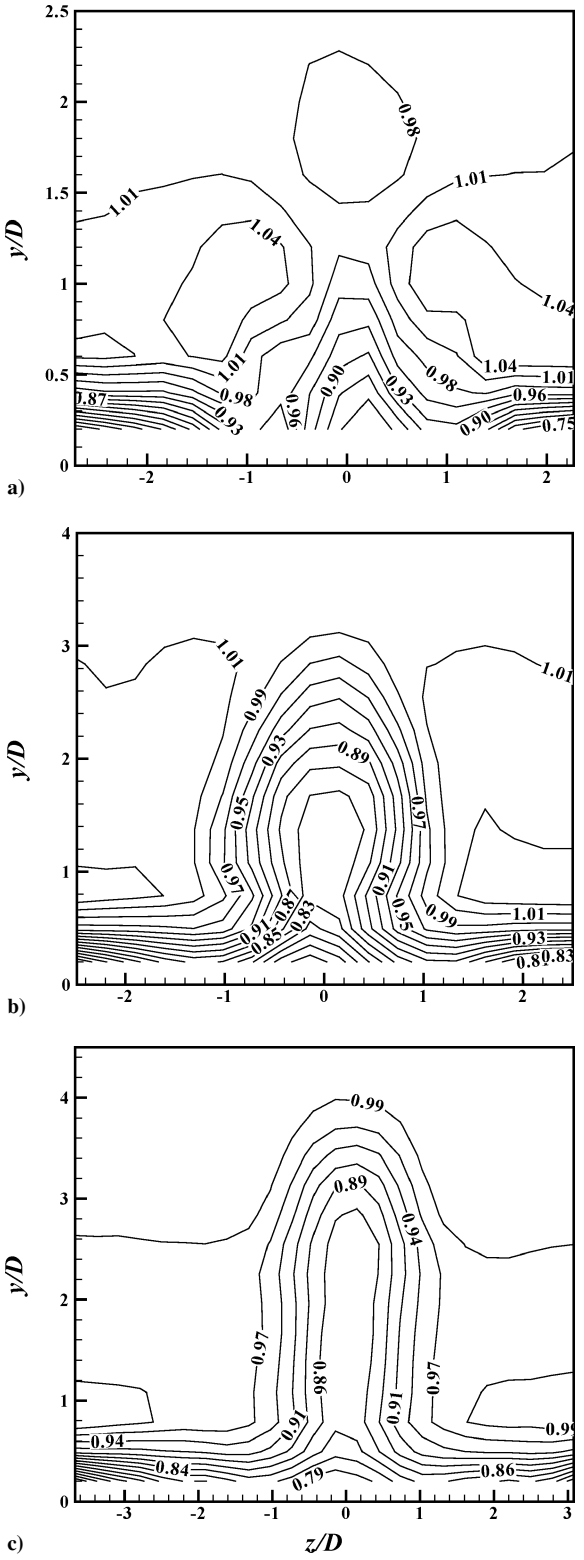

Fig. 15 Streamwise mean velocity contours for SJCF from clustered orifice: a) $x/D = 0.5$, b) $x/D = 5$, and c) $x/D = 10$.

for brevity) also exhibited somewhat higher penetration for the tapered orifice. However, the difference was minor, and the tapered configuration was not pursued any further in this study.

The velocities in Fig. 13 are the smallest for the pitched orifice. This is mainly because of the resonance characteristics of the cavity-orifice configuration. All data are for a driving frequency of 25 Hz. For the cylindrical, tapered, and clustered orifices this corresponded to the Helmholtz resonance (Sec. II). For the pitched orifice, because of the increased length, the resonance frequency was lower, about 18 Hz. Therefore, the response was less pronounced for the pitched case as a result of off-resonant condition. (The Helmholtz resonance simply provides a means to impart large-amplitude perturbation. The synthetic jet characteristics are governed by the stroke length L_0/D and momentum-flux ratio J regardless of the resonance condition.)

Data presented in the rest of the paper pertain to a frequency, $f = 25$ Hz, and input voltage, $A = 9.6$ V. The resulting stroke length

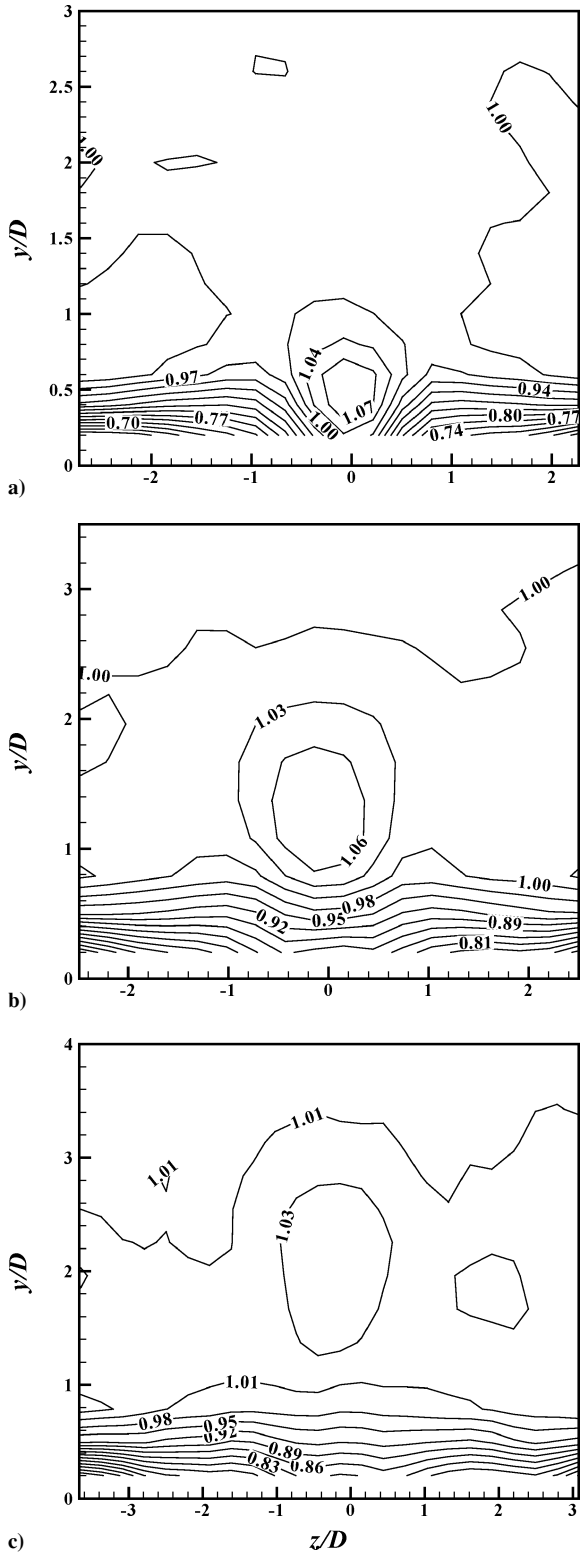

Fig. 16 Streamwise mean velocity contours for SJCF from pitched orifice: a) $x/D = 0.5$, b) $x/D = 5$, and c) $x/D = 10$.

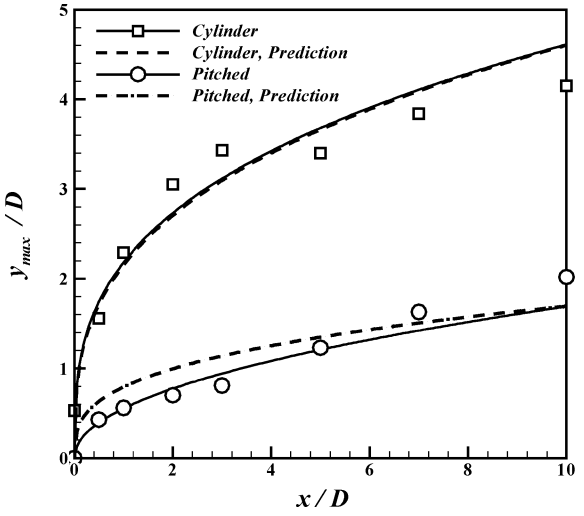

Fig. 17 SJCF trajectories for cylindrical and pitched cases: $z/D = 0$.

and momentum-flux ratio are 19.9 and 6, respectively. The mean velocity distribution for the cylindrical case is shown in Fig. 14 for $x/D = 0.5$ and 10. These together with data at $x/D = 5$ (Fig. 9a) illustrate the evolution of the round SJCF issuing normally to the crossflow. A kidney-shaped distribution of high-velocity fluid is observed at the location closest to the exit. However, farther downstream the flowfield is characterized mainly by the dome of low-velocity fluid pulled from the boundary layer.

A similar evolution is seen for the clustered case, shown in Fig. 15. Once again, the clustered configuration is remarkable in that the effect from the nine orifices becomes an aggregate, as if the SJ were issuing from a single orifice. In comparison with the cylindrical case, the jet penetration is somewhat lower, and the lateral spreading at the farthest downstream location is actually smaller although the holes are distributed over a larger area. A brief survey was also conducted for a cluster of nine orifices with doubled orifice spacing; those data are not shown for brevity. Increased spacing resulted in the lower jet penetration. For example, at $x/D = 10$, the $U/U_\infty = 0.99$ contour reached up to $y/D = 2.8$ instead of about 4 seen in Fig. 15c. The mean velocity distribution still exhibited a cellular structure at $x/D = 5$. Thus, the streamwise location where the flowfield becomes an aggregate is farther with larger orifice spacing.

The corresponding velocity distributions for the pitched case are presented in Fig. 16. There is a noteworthy difference with the other two configurations. Instead of a dome of low-velocity fluid, a higher-velocity core is observed around the symmetry plane, near the wall. Even at $x/D = 10$ this core has neither lifted up nor distorted into the kidney shape. It is apparent that the jet pitched at 20 deg behaves similar to a wall-jet,[37] within the measurement domain covered in the experiment. The JICF from a 20-deg pitched orifice also exhibits a high-velocity core near the wall.[29] Thus, there is a similarity between SJCF and JICF for the pitched case too.

The jet trajectories, based on $y_{\max}$ location, as discussed in Sec. III.B, are shown in Fig. 17 for the normal and pitched orifices. These data were obtained by measuring $u'_f(y)$ profiles at different downstream locations on the symmetry plane. The symbols represent the data, the solid lines are curve fit through the data, while the dashed lines indicate predictions of Eq. (4). It is clear that with the chosen definitions the trajectories of a SJCF and a JICF, for the ranges of Stokes and Reynolds numbers covered, are practically identical. The peaks in u'_f profiles for the clustered case became obscure shortly downstream of the orifice, and thus the corresponding trajectory could not be shown. However, comparison of Figs. 15 and 14, as stated earlier, makes it clear that the penetration for the clustered case is somewhat lower.

Distributions of phase-averaged properties were obtained with the same $\times$-wire survey scheme using the input to the woofer as a reference. The zero crossings of the reference signal with positive slopes were used as triggers. Data were acquired for 19 phases within the period of perturbation. Phase-averaged streamwise velocity contours at $x/D = 5$ are shown for the cylindrical case in Fig. 18. The eight figures are approximately at equal intervals covering the period. The phases on the left represent the discharge segment of the cycle, whereas those on the right represent suction. These data capture the unsteady cycling of the synthetic jet in the

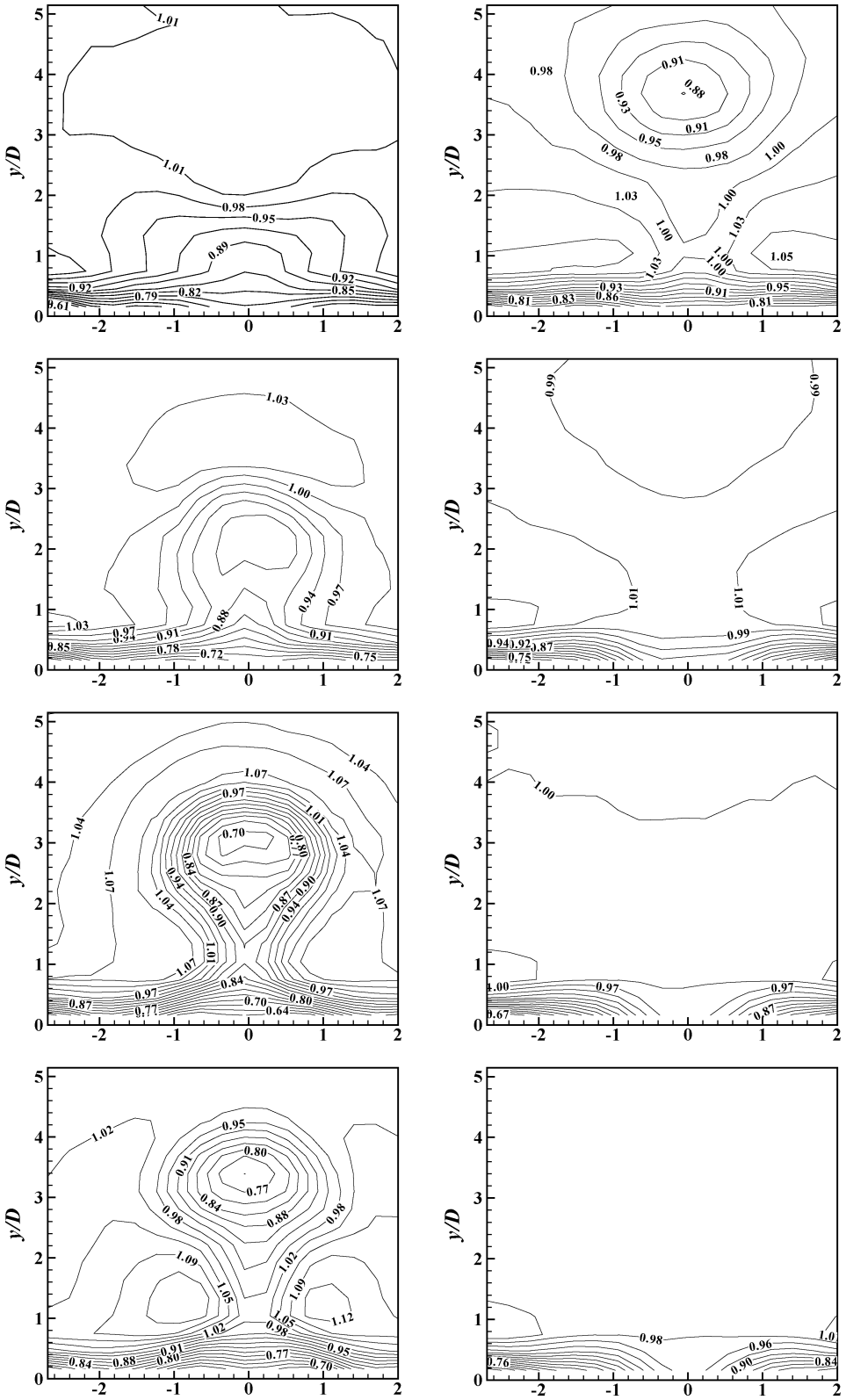

Fig. 18 Phase-averaged streamwise velocity contours for SJCF from cylindrical orifice: $x/D = 5$. The eight figures are at equally spaced phases within the excitation period.

crossflow and provide a clear perspective of the events leading to the time-averaged field seen in Fig. 9a. An inspection reveals that the phase-averaged velocity goes through the largest changes at about $y/D = 3.5$ on the symmetry plane ($z = 0$), with varying phase over the period. This gives rise to the peak in the u'_f profile discussed in Sec. III.B. Corresponding streamwise vorticity data,[30] not shown here, featured the bound vortex pair during the discharge phase only. However, a vortex pair of opposite sense occurred close to the wall at all phases. The latter, apparently caused by reorientation of the approach boundary layer, gave rise to the conspicuous vortex pair of opposite sense near the wall seen in Fig. 9b. Matching phase-averaged data for the clustered case are shown in Fig. 19. One notes somewhat complex changes in the flowfield within the cycle. Compared to the cylindrical case, the events take place closer to the wall leading to a lesser penetration of the SJCF on a time-averaged basis (Fig. 15b).

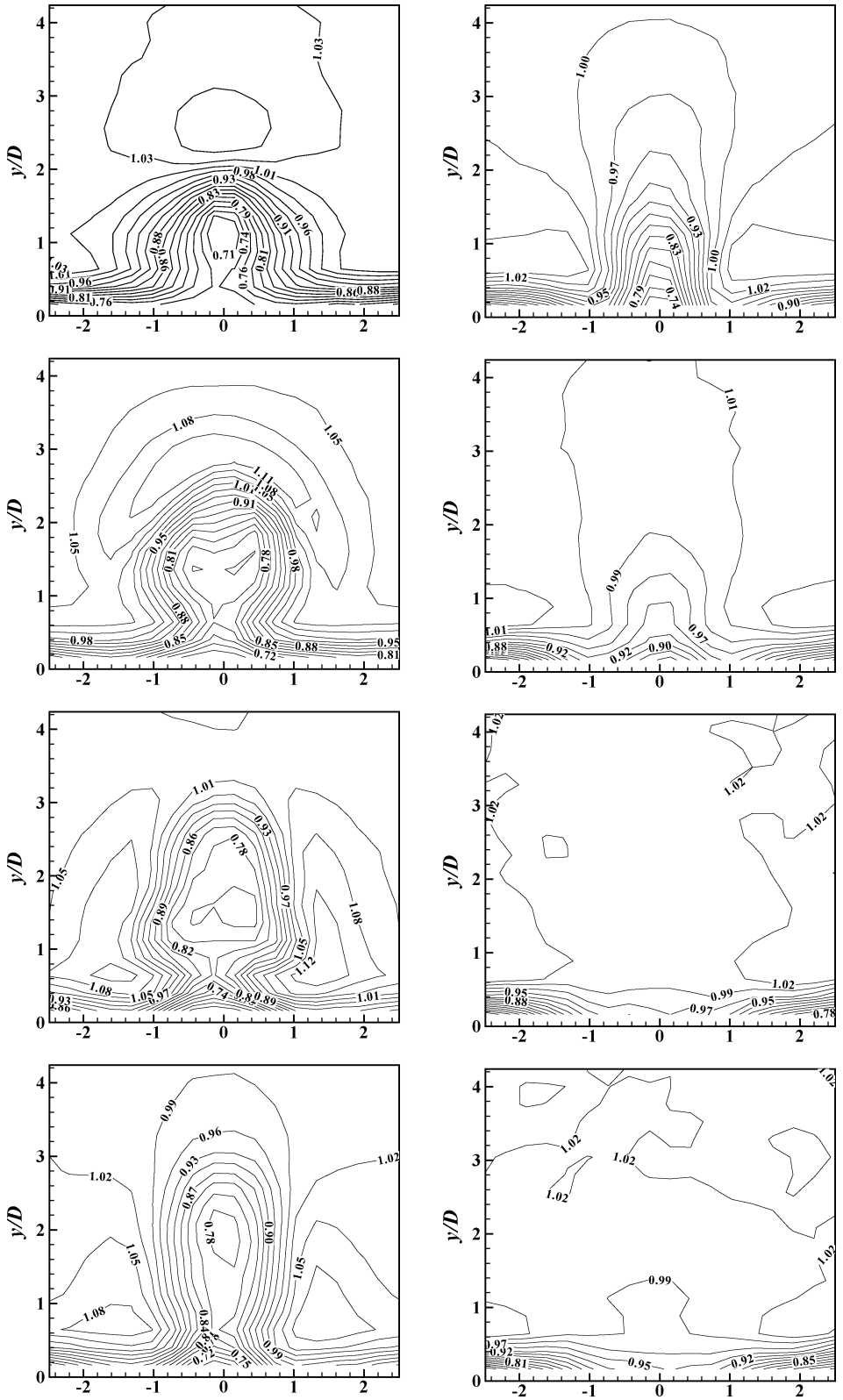

Fig. 19 Phase-averaged streamwise velocity contours as in Fig. 18 for the cluster case.

IV. Conclusions

Results of an experimental investigation on synthetic jets are presented. The main conclusions are enumerated in the following:

1) For the parameter range covered, the threshold for the formation of synthetic jet without crossflow is about $L_0/D = 0.25$. A SJ is not formed at lower L_0/D.

2) There is an upper threshold of about $L_0/D = 5$ above which the profiles of normalized centerline mean velocity become invariant. This upper threshold might have a connection with the phenomenon of saturation of impulsively generated vortices.

3) For a given frequency and U_∞, the penetration height $y_{\max}$ of a SJCF increases with increasing stroke length L_0/D. However, unlike various other properties, $y_{\max}$ is not a unique function of L_0/D.

4) It is found that $y_{\max}$ at a given streamwise location solely depends on the momentum-flux ratio. For the present incompressible

flow, when this ratio is defined as $J = (V_{\max}/U_{\infty})^2$, not only all of the penetration height data collapse but also the trajectories are predicted well by correlation equations for steady jets in crossflow.

5) Mean velocity, streamwise vorticity, as well as turbulence intensity distributions for a SJCF, are found to be similar to those of a steady JICF. A pair of counter-rotating streamwise vortices, resembling the bound vortex pair of a JICF, is clearly observed. Mean velocity for normal injection exhibits the dome of low-momentum fluid pulled up from the boundary layer. The entire domain is characterized by high turbulence intensity.

6) Just a few equivalent diameters downstream, the SJCF from the cluster of orifices is found to be quite similar to that from the single orifice. Jet penetration is somewhat less for the cluster in comparison to the single orifice case as a result of increased mixing with the crossflow. With larger spacing of the orifices in the cluster, jet penetration becomes even lower.

7) Although the mean velocity distribution for normal injection is characterized by a dome of low-momentum fluid, the pitched case involves a region of high-momentum fluid occurring near the wall and around the symmetry plane, similar to a wall jet. As expected, the jet penetration is the least for the pitched geometry.

Acknowledgments

The work was supported by the NASA–OAI Collaborative Aerospace Research and Fellowship Program. The second author is grateful to Connecticut Space Grant College Consortium–EPSCoR Core Funding for providing support. The authors are also thankful to Gerard E. Welch of the U.S. Army for valuable input.

References

[1]Smith, B. L., and Glezer, A., "The Formation and Evolution of Synthetic Jets," *Physics of Fluids*, Vol. 10, No. 9, 1998, pp. 2281–2297.

[2]Ingard, U., and Labate, S., "Acoustic Circulation Effects and the Nonlinear Impedance of Orifices," *Journal of the Acoustical Society of America*, Vol. 174, No. 1, 1950, pp. 211–218.

[3]Lighthill, M. J., "Acoustic Streaming," *Journal of Sound and Vibration,* Vol. 61, No. 3, 1978, pp. 391–418.

[4]Utturkar, Y., Holman, R., Mittal, R., Carroll, B., Sheplak, M., and Cattafesta, L., "A Jet Formation Criterion for Synthetic Jet Actuators," AIAA Paper 2003-0636, Jan. 2003.

[5]Carter, J., and Soria, J., "The Evolution of Round Zero-Net-Mass-Flux Jets," *Journal of Fluid Mechanics*, Vol. 472, 2002, pp. 167–200.

[6]Bera, J. C., Michard, M., Grosjean, N., and Comte-Bellot, G., "Flow Analysis of Two-Dimensional Pulsed Jets by Particle Image Velocimetry," *Experiments in Fluids*, Vol. 31, No. 5, 2001, pp. 519–532.

[7]Smith, B. L., and Swift, G. W., "A Comparison Between Synthetic Jets and Continuous Jets," *Experiments in Fluids*, Vol. 34, No. 4, 2003, pp. 467–472.

[8]Smith, D. R., Amitay, M., Kibens, Parekh, D. E., and Glezer, A., "Modification of Lifting Body Aerodynamics Using Synthetic Jet Actuators," AIAA Paper 98-0209, Jan. 1998.

[9]Amitay, M., Smith, B. L., and Glezer, A., "Aerodynamic Flow Control Using Synthetic Jet Technology," AIAA Paper 98-0208, Jan. 1998.

[10]Amitay, M., Kibens, V., Parekh, D. E., and Glezer, A., "Flow Reattachment Dynamics over a Thick Airfoil Controlled by Synthetic Jet Actuators," AIAA Paper 99-1001, Jan. 1999.

[11]Amitay, M., Smith, D. R., Kibens, V., Parekh, D. E., and Glezer, A., "Modification of the Aerodynamics Characteristics of an Unconventional Airfoil Using Synthetic Jet Actuators," *AIAA Journal*, Vol. 39, No. 3, 2001, pp. 361–370.

[12]Honohan, A. M., Amitay, M., and Glezer, A., "Aerodynamic Control Using Synthetic Jets," AIAA Paper 2000-2401, June 2000.

[13]Smith, B. L., and Glezer, A., "Jet Vectoring Using Synthetic Jets," *Journal of Fluid Mechanics*, Vol. 458, 2002, pp. 1–34.

[14]Amitay, M., Honohan, A., Trautman, M., and Glezer, A., "Modification of the Aerodynamic Characteristics of Bluff Bodies Using Fluidic Actuators," AIAA Paper 97-2004, June 1997.

[15]Chen, Y., Liang, S., Aung, K., Glezer, A., and Jagoda, J., "Enhanced Mixing in a Simulated Combustor Using Synthetic Jet Actuators," AIAA Paper 99-0449, Jan. 1999.

[16]Amitay, M., Pitt, D., and Glezer, A., "Separation Control in Duct Flows," *Journal of Aircraft*, Vol. 39, No. 4, 2002, pp. 616–620.

[17]Liu, Z., Sankar, L. N., and Hassan, A. A., "Alteration of the Tip Vortex Structure of a Hovering Rotor Using Oscillatory Jet Excitation," AIAA Paper 99-0906, Jan. 1999.

[18]McCormack, D. C., "Boundary Layer Separation Control with Directed Synthetic Jets," AIAA Paper 2000-0519, Jan. 2000.

[19]Gilarranz, J. L., Traub, L. W., and Rediniotis, O. K., "Characterization of a Compact, High-Power Synthetic Jet Actuator for Flow Separation Control," AIAA Paper 2002-0127, Jan. 2002.

[20]Grossman, K., Bohdan, C., and Vanwie, D., "Sparkjet Actuators for Flow Control," AIAA Paper 2003-0057, Jan. 2003.

[21]Chen, Y., Liang, S., Aung, K., Glezer, A., and Jagoda, J., "Enhanced Mixing in a Simulated Combustor Using Synthetic Jet Actuators," AIAA Paper 99-0449, Jan. 1999.

[22]Smith, D. R., Kibens, V., Pitt, D. M., and Hopkins, M. A., "Effect of Synthetic Jet Arrays on Boundary Layer Control," *SPIE Proceedings*, Vol. 3674, July 1999, pp. 401–409.

[23]Bridges, A., and Smith, D. R., "Influence of Orifice Orientation on a Synthetic Jet-Boundary-Layer Interaction," *AIAA Journal*, Vol. 41, No. 12, 2003, pp. 2394–2402.

[24]Smith, D. R., "Interaction of a Synthetic Jet with a Crossflow Boundary Layer," *AIAA Journal*, Vol. 40, No. 11, 2002, pp. 2277–2288.

[25]Gordon, M., and Soria, J., "PIV Measurements of a Zero-Net-Mass-Flux Jet in Cross Flow," *Experiments in Fluids*, Vol. 33, No. 6, 2002, pp. 863–872.

[26]Smith, B., Trautman, M., and Glezer, A., "Controlled Interactions of Adjacent Synthetic Jets," AIAA Paper 99-0669, Jan. 1999.

[27]Watson, M., Jaworski, A. J., and Wood, N. J., "Contribution to the Understanding of Flow Interactions Between Multiple Synthetic Jets," *AIAA Journal*, Vol. 41, No. 4, 2003, pp. 747–749.

[28]Anderson, J. S., "The Effect of an Air Flow on a Single Side Branch Helmholtz Resonator in a Circular Duct," *Journal of Sound and Vibration*, Vol. 52, No. 3, 1977, pp. 423–431.

[29]Milanovic, I. M., and Zaman, K. B. M. Q., "Fluid Dynamics of Highly Pitched and Yawed Jets in Crossflow," *AIAA Journal*, Vol. 42, No. 5, 2004, pp. 874–883.

[30]Zaman, K. B. M. Q., and Milanovic, I. M., "Synthetic Jets in Cross-Flow. Part 1: Round Jet," AIAA Paper 03-3714, June 2003.

[31]Milanovic, I. M., and Zaman, K. B. M. Q., "Synthetic Jets in Cross-Flow. Part 2: Jets from Orifices of Different Geometry," AIAA Paper 2003-3715, June 2003.

[32]Gharib, M., Rambod, E., and Shariff, K., "A Universal Time Scale for Vortex Ring Formation," *Journal of Fluid Mechanics*, Vol. 360, 1998, pp. 121–140.

[33]Krueger, P. S., and Gharib, M., "The Significance of Vortex Ring Formation to the Impulse and Thrust of a Starting Jet," *Physics of Fluids*, Vol. 15, No. 5, 2003, pp. 1271–1281.

[34]Abramovich, G. N., *The Theory of Turbulent Jets*, MIT Press, Cambridge, MA, 1963.

[35]Zaman, K. B. M. Q., and Foss, J. K., "The Effect of Vortex Generators on a Jet in a Cross-Flow," *Physics of Fluids*, Vol. 9, No. 1, 1997, pp. 106–114.

[36]Gopalan, S., Abraham, B., and Katz, J., "Turbulent Jet Injected into a Cross Flow—Analysis of the Flow Structure and Wall Pressure Fluctuations," American Society of Mechanical Engineers, Paper FEDSM2002-31420, July 2002.

[37]Visbal, M. R., Gaitonde, D. V., and Gogineni, S., "Direct Numerical Simulation of a Forced Transitional Plane Wall Jet," AIAA Paper 98-2643, June 1998.

H. Reed
Associate Editor